Inorganic Chemistry

Forum Article

pubs.acs.org/IC

N_2 Activation by an Iron Complex with a Strong Electron-Donating Iminophosphorane Ligand

Tatsuya Suzuki,[†,‡] Yuko Wasada-Tsutsui,[†] Takahiko Ogawa,[†] Tomohiko Inomata,[†] Tomohiro Ozawa,[†] Yoichi Sakai,[§] Michael D. Fryzuk,*[,‡] and Hideki Masuda*[,†]

[†]Department of Frontier Materials, Graduate School of Engineering, Nagoya Institute of Technology, Gokiso, Showa, Nagoya 466-8555, Japan

[‡]Department of Chemistry, The University of British Columbia, 2036 Main Mall, Vancouver, British Columbia, Canada V6T 1Z1

[§]Department of Chemistry, Daido University, Takiharu-cho, Minami-ku, Nagoya 457-8530, Japan

Supporting Information

ABSTRACT: A new tridentate cyclopentane-bridged iminophosphorane ligand, *N*-(2-diisopropylphosphinophenyl)-*P*,*P*-diisopropyl-*P*-(2-(2,6-diisopropylphenylamido)cyclopent-1-enyl)phosphoranimine ($NpNP^{iPr}$), was synthesized and used in the preparation of a diiron dinitrogen complex. The reaction of the iron complex $FeBr(NpNP^{iPr})$ with KC_8 under dinitrogen yielded the dinuclear dinitrogen Fe complex $[Fe(NpNP^{iPr})]_2(\mu\text{-}N_2)$, which was characterized by X-ray analysis and resonance Raman and NMR spectroscopies. The X-ray analysis revealed a diiron complex bridged by the dinitrogen molecule, with each metal center coordinated by an $NpNP^{iPr}$ ligand and dinitrogen in a trigonal-monopyramidal geometry. The N−N bond length is 1.184(6) Å, and resonance Raman spectra indicate that the N−N stretching mode $\nu(^{14}N_2/^{15}N_2)$ is 1755/1700 cm^{-1}. The magnetic moment of $[Fe(NpNP^{iPr})]_2(\mu\text{-}N_2)$ in benzene-d_6 solution, as measured by ^1H NMR spectroscopy by the Evans method, is 6.91μ_B (S = 3). The Mössbauer spectrum at 78 K showed δ = 0.73 mm/s and ΔE_Q = 1.83 mm/s. These findings suggest that the iron ions are divalent with a high-spin configuration and that the N_2 molecule has $(N{=}N)^{2-}$ character. Density functional theory calculations performed on $[Fe(NpNP^{iPr})]_2(\mu\text{-}N_2)$ also suggested that the iron is in a high-spin divalent state and that the coordinated dinitrogen molecule is effectively activated by π back-donation from the two iron ions (dπ) to the dinitrogen molecule (π_x^* and π_y^*). This is supported by cooperation between a large negative charge on the iminophosphorane ligand and strong electron donation and effective orbital overlap between the iron dπ orbitals and N_2 π^* orbitals supplied by the phosphine ligand.

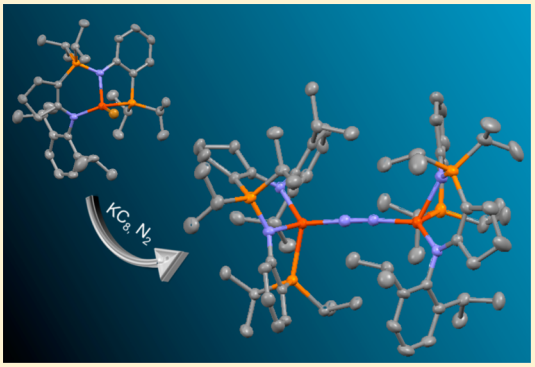

INTRODUCTION

The first dinitrogen metal complex was identified as $[Ru(NH_3)_5(N_2)]^{2+}$ by Allen and Senoff in 1965.[1] Subsequently, a wide variety of transition-metal complexes with coordinated dinitrogen have been studied by inorganic and organometallic chemists.[2] The chemical conversion of N_2 to ammonia promoted by a well-defined catalyst precursor has also been studied using mainly Mo and Fe complexes from the viewpoint of the structure−function relationships identified in the nitrogenase FeMoco active center (which includes Fe and Mo).[3] In this context, molybdenum dinitrogen complexes have been studied and examples of crystal structures have been reported.[4] Catalytic conversion of dinitrogen to ammonia by molybdenum complexes has been investigated mainly by Schrock[5] and Nishibayashi.[6] Capture and activation of dinitrogen using base-metal complexes have been studied by the groups of Chirik,[7] Holland,[8] and Peters[9] using low-valent iron and cobalt complexes.

Additionally, Holland and co-workers recently published a report indicating that the three- and four-coordinate iron−N_2 complexes with β-diketiminate ligands (nacnac), which have a low coordination number for the iron centers with coordinated N_2, similar to that suggested in the nitrogenase active site of FeMoco, activate N_2 more effectively than five- or six-coordinate iron−N_2 complexes.[8d,e] These reports suggest that a coordinatively unsaturated electron-rich iron complex can effectively capture and activate dinitrogen.

The coordinated dinitrogen molecule in dinitrogen-bridged diiron complexes can in general be formally considered as either a neutral N_2 or as a N_2^{2-} dianion, depending whether π back-bonding from the metal to the dinitrogen moiety is operative. Thus, the coordinated dinitrogen molecule can be activated if the metal ion is stabilized by a strong σ-donating ancillary ligand system, which in turn enhances overlap of the metal dπ and dinitrogen π^* orbitals. Recently, Peters and co-

Special Issue: Small Molecule Activation: From Biological Principles to Energy Applications

Received: March 11, 2015
Published: July 2, 2015

DOI: 10.1021/acs.inorgchem.5b00536
Inorg. Chem. 2015, 54, 9271−9281

Scheme 1. Synthesis of LiNpNP^{iPr} and HNpNP^{iPr}

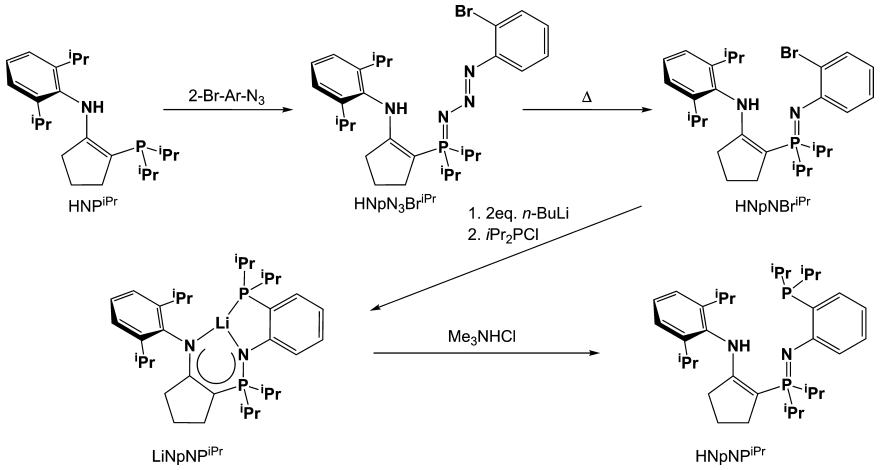

workers investigated iron complexes with tris(phosphino)silyl, bis(phosphino)(thioether)silyl, and bis(thioether)(phosphino)-silyl ligands.[9b] The former two mononuclear iron(II) complexes were found to bind dinitrogen, while the bis-(thioether)(phosphino)silyl ligands could not. Instead, it was found that the latter complex traps dinitrogen in the presence of hydride anion. These findings indicate that strong σ donation from the ancillary ligands to the metal ion is essential to facilitate capture of dinitrogen.

Building on the above findings, in this paper we describe the design and synthesis of a new tridentate NpNP ligand, *N*-(2-diisopropylphosphinophenyl)-*P*,*P*-diisopropyl-*P*-(2-(2,6-diisopropylphenylamido)cyclopent-1-enyl)phosphoranimine (NpNP^{iPr}), that incorporates an iminophosphorane unit (R_3−P═N−R), an electron-rich phosphine, and an aryl imine. This combination was chosen to mimic the nacnac donor set by the combination of the imine and iminophosphorane moieties[10] and enhance it by the presence of the phosphine donor. We anticipated that this combination of donors would provide an electron-rich metal center, which in turn would allow increased activation of the dinitrogen moiety upon coordination. We also report the synthesis and characterization of a formally monovalent diiron(I) dinitrogen complex with NpNP^{iPr} and discuss the activation of the coordinated dinitrogen.

RESULTS AND DISCUSSION

Synthesis and Characterization of the HNpNP^{iPr} Ligand and the LiNpNP^{iPr} Complex. The synthesis of the compounds HNpNP^{iPr} and LiNpNP^{iPr} is illustrated in Scheme 1. The cyclopentylidene-based phosphine−amine starting material 2,6-diisopropyl-*N*-(2-diisopropylphosphinocyclopentylidene)aniline (HNP^{iPr}), which contains a bulky 2,6-diisopropylphenyl group on the amine nitrogen, was synthesized according to literature procedures.[11] The reaction of HNP^{iPr} with 2-bromophenyl azide (2-Br-Ar-N_3) gave the phosphazide HNpN$_3$Br^{iPr} in high yield as previously reported.[12] Subsequent heating of the product at 80 °C overnight produced the iminophosphorane HNpNBr^{iPr} in excellent high yield. The reaction of HNpNBr^{iPr} with 2 equiv of *n*-BuLi followed by the reaction with iPr_2PCl yielded LiNpNP^{iPr}. The crystal structure of LiNpNP^{iPr} is shown in Figure 1. The lithium salt was protonated with Me_3NHCl in tetrahydrofuran (THF) to form the neutral ligand HNpNP^{iPr}. Colorless block crystals of HNpNP^{iPr} were obtained after storage at −35 °C. The crystal

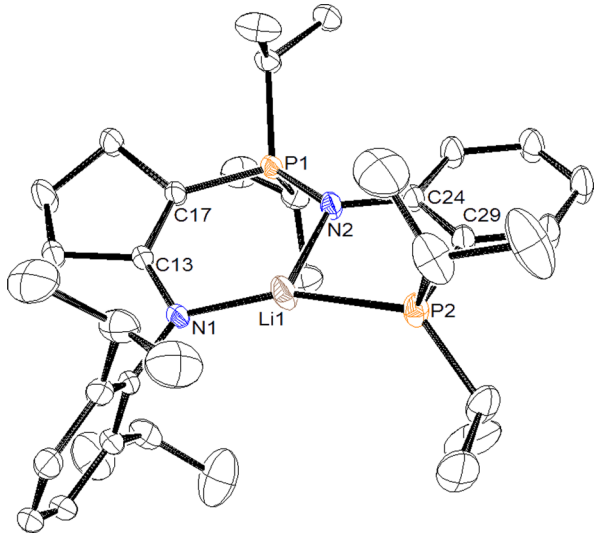

Figure 1. ORTEP drawing of the crystal structure of LiNpNPiPr with ellipsoids at the 30% probability level. All hydrogen atoms have been omitted for clarity. Selected bond lengths (Å) and angles (deg): P(1)−N(2) 1.6202(13), P(1)−C(17) 1.757(2), P(2)−C(29) 1.825(3), N(1)−C(13) 1.3348(19), N(2)−C(24) 1.398(3), C(13)−C(17) 1.395(3), C(24)−C(29) 1.421(2), N(1)−C(13)−C(17) 129.10(16), P(1)−C(17)−C(13) 131.57(11), N(2)−P(1)−C(17) 110.53(9), P(1)−N(2)−C(24) 125.75(14), N(2)−C(24)−C(29) 119.55(18), P(2)−C(29)−C(24) 118.95(14), P(2)−Li(1)−N(1) 155.4(2), P(2)−Li(1)−N(2) 87.56(15), N(1)−Li(1)−N(2) 117.03(17).

structure of HNpNP^{iPr}, which contains two independent HNpNP^{iPr} molecules in the unit cell, is shown in Figure 2. In the crystal structure of LiNpNP^{iPr} (Figure 1), the lithium ion is coordinated to the anilide nitrogen, the phosphine phosphorus, and the phosphoranimine nitrogen of NpNP^{iPr} to form a trigonal plane. The sum of the bond angles at the lithium ion is close to 360° (P(2)−Li(1)−N(1) = 155.4(2)°, P(2)−Li(1)−N(2) = 87.56(15)°, N(1)−Li(1)−N(2) = 117.03(17)°). The molecular structure of the protonated derivative HNpNP^{iPr} is bent from the N−P−N plane containing the cyclopentyl ring, although it is essentially the same as the structure of LiNpNP^{iPr}. This indicates that the π electrons in the N−P−N ring in LiNpNP^{iPr} are delocalized compared with the π electrons of HNpNP^{iPr}, which adopts the enamine tautomeric form. This interpretation is supported by the bond lengths of the NpNP^{iPr}

DOI: 10.1021/acs.inorgchem.5b00536
Inorg. Chem. 2015, 54, 9271−9281

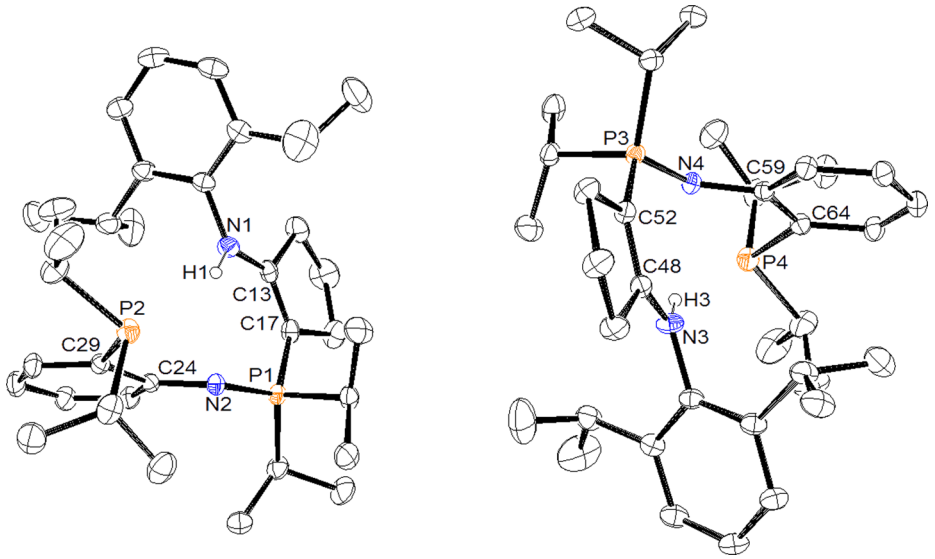

Figure 2. ORTEP drawing of the crystal structure of HNpNP^{iPr} with ellipsoids at the 30% probability level. All hydrogen atoms except for H(1) and H(3) have been omitted for clarity. Selected bond lengths (Å) and angles (deg): P(1)−N(2) 1.5855(11), P(1)−C(17) 1.7726(17), P(2)−C(29) 1.839(3), P(3)−N(4) 1.5900(11), P(3)−C(52) 1.7687(15), P(4)−C(64) 1.837(3), N(1)−C(13) 1.3609(19), N(2)−C(24) 1.383(3), N(3)−C(48) 1.3570(18), N(4)−C(59) 1.385(3), C(13)−C(17) 1.364(3), C(24)−C(29) 1.4222(19), C(48)−C(52) 1.362(2), C(59)−C(64) 1.4172(19), N(1)−C(13)−C(17) 128.20(15), P(1)−C(17)−C(13) 124.24(11), N(2)−P(1)−C(17) 113.82(7), P(1)−N(2)−C(24) 128.13(13), N(2)−C(24)−C(29) 118.06(18), P(2)−C(29)−C(24) 117.81(15), N(3)−C(48)−C(52) 128.14(14), P(3)−C(52)−C(48) 123.56(11), N(4)−P(3)−C(52) 113.50(7), P(3)−N(4)−C(59) 126.72(13), N(4)−C(59)−C(64) 117.99(17), P(4)−C(64)−C(59) 117.21(15).

Scheme 2. Synthesis of the Iron Complex with the NpNP^{iPr} Ligand and Reduction To Generate the Dinitrogen Complex

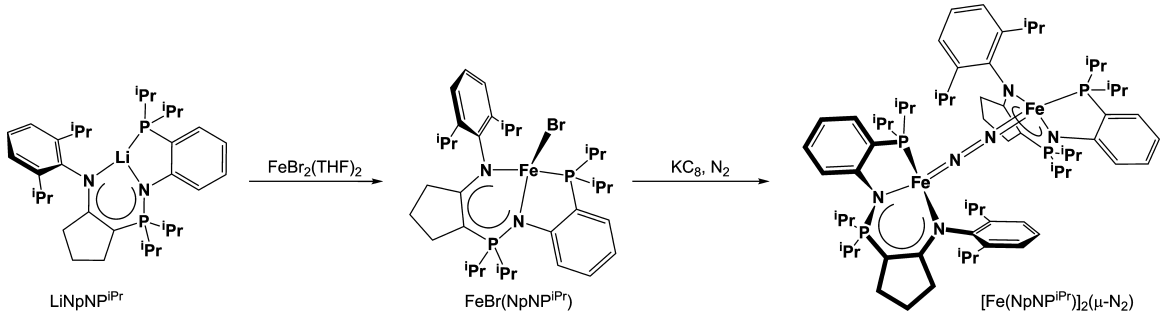

ligands of LiNpNP^{iPr} and HNpNP^{iPr} as follows; for LiNpNP^{iPr}, the P(1)−N(2), P(1)−C(17), C(17)−C(13), and N(1)−C(13) bond lengths are 1.6202(13), 1.757(2), 1.395(3), and 1.335(2) Å, respectively, while for HNpNP^{iPr}, the P(1)−N(2)/P(3)−N(4), P(1)−C(17)/P(3)−C(52), C(17)−C(13)/C(52)−C(48), and N(1)−C(13)/N(3)−C(48) bond lengths are 1.5855(1)/1.5900(11), 1.7726(17)/1.7687(15), 1.364(3)/1.362(2), and 1.3609(19)/1.3570(18) Å, respectively. Furthermore, for compound HNpNP^{iPr}, a hydrogen bond extends between the enamine NH and the phosphoranimine (N(1)···N(2)/N(3)···N(4) = 3.006/2.990 Å), which likely stabilizes the enamine tautomer. Evidence for this is also provided by the ^{1}H and ^{31}P NMR spectra of HNpNP^{iPr} (Figures S3 and S4 in the Supporting Information), which show that there is only one species present in solution.

Preparation and Characterization of the Fe(II) Complex with the NpNP^{iPr} Ligand. Treatment of the lithium salt LiNpNP^{iPr} with $FeBr_2(THF)_2$ in Et_2O yielded the iron bromide complex FeBr(NpNP^{iPr}), which acts as a precursor to the diiron dinitrogen complex, as shown in Scheme 2. The iron monobromide complex could be obtained as single crystals suitable for X-ray analysis. The crystal structure of FeBr(NpNP^{iPr}) (Figure 3) revealed a distorted trigonal-monopyramidal geometry (τ = 0.64; the value of τ was calculated by using eq 1 in the Experimental Section)[13] with the Br, anilide nitrogen, and phosphine in the basal plane and the phosphoranimine nitrogen at the apex. The sum of the angles in the basal trigonal plane is 353.0° (i.e., close to 360°) (Br(1)−Fe(1)−N(1) = 121.06(5)°, Br(1)−Fe(1)−P(2) = 113.575(14)°, and P(2)−Fe(1)−N(1) = 118.29(5)°). The average angle of the axial ligands from the basal plane is close to 90° (N(2)−Fe(1)−Br(1) = 109.24(5)°, N(2)−Fe(1)−N(1) = 102.49(7)°, and N(2)−Fe(1)−P(2) = 83.67(5)°). The bond lengths between the ligands and the metal in FeBr(NpNP^{iPr}) are Fe(1)−Br(1) = 2.4323(4), Fe(1)−P(2) = 2.4037(5), and Fe(1)−N(1) = 2.0004(16) for the basal plane and Fe(1)−N(2) = 2.0515(19) Å for the axial ligand. These bond lengths and the geometry at the metal center are very similar to those of a previously reported high-spin Fe(II) complex with a pyridine-linked bis(anilide) pincer ligand.[14] The π electrons of the ligand backbone are also delocalized on the N−P−N ring, as understood from the bond lengths (P(1)−N(2) = 1.6275(14), P(1)−C(17) = 1.769(2), C(17)−C(13) = 1.384(4), and N(1)−C(13) = 1.362(3) Å). As expected, the

DOI: 10.1021/acs.inorgchem.5b00536
Inorg. Chem. 2015, 54, 9271−9281

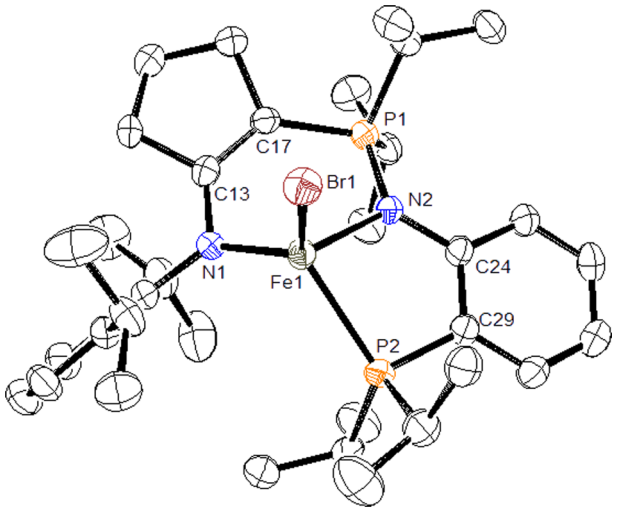

Figure 3. ORTEP drawing of the crystal structure of FeBr(NpNP^{iPr}) with ellipsoids at the 30% probability level. All hydrogen atoms have been omitted for clarity. Selected bond lengths (Å) and angles (deg): Br(1)−Fe(1) 2.4323(4), Fe(1)−P(2) 2.4037(5), Fe(1)−N(1) 2.0004(16), Fe(1)−N(2) 2.0515(19), P(1)−N(2) 1.6275(14), P(1)−C(17) 1.769(2), C(13)−C(17) 1.384(4), C(24)−C(29) 1.417(3), P(2)−C(29) 1.812(3), Br(1)−Fe(1)−P(2) 113.575(14), Br(1)−Fe(1)−N(1) 121.06(5), Br(1)−Fe(1)−N(2) 109.24(5), P(2)−Fe(1)−N(1) 118.29(5), P(2)−Fe(1)−N(2) 83.67(5), N(1)−Fe(1)−N(2) 102.49(7).

^{1}H NMR spectra of FeBr(NpNP^{iPr}) in C_6D_6 included broadened signals in the paramagnetic region (Figure S5). The magnetic moment of FeBr(NpNP^{iPr}) in the solution state, as measured by the Evans method,[15] was found to be μ_{eff} = 5.06μ_B, which indicates that the complex is paramagnetic and has four unpaired electrons, consistent with high-spin Fe(II).

Preparation and Characterization of the Diiron Dinitrogen Complex. Reduction of the iron(II) bromide complex FeBr(NpNP^{iPr}) with KC_8 under a dinitrogen atmosphere produced a color change from yellow to dark brown. Fortunately, we obtained dark-red single crystals under a dinitrogen atmosphere from *n*-pentane, which were found to be highly sensitive to air. X-ray crystal structure analysis revealed a dinuclear iron complex bridged by μ-N_2, [Fe(NpNP^{iPr})]$_2$(μ-N_2) (Figure 4). In the crystal structure, the two iron sites were found to be rotated with respect to each other about the μ-N_2 molecule with a N(2)−Fe(1)−Fe(2)−N(4) torsion angle of 92.07°. Each iron complex has a distorted trigonal-monopyramidal geometry (τ = 0.64 and 0.65 for Fe(1) and Fe(2), respectively) with the μ-N_2 nitrogen, anilide nitrogen, and phosphine phosphorus atoms in the basal trigonal plane and the phosphoranimine nitrogen at the apex. For the Fe(1) site, the sum of the angles in the basal plane, 353.02°, is close to 360° (N(5)−Fe(1)−N(1) = 122.33(16)°, N(5)−Fe(1)−P(2) = 104.55(13)°, and P(2)−Fe(1)−N(1) = 126.14(14)°). The average angle of the axial ligand from the basal plane is close to 90° (N(2)−Fe(1)−N(5) = 116.23(17), N(2)−Fe(1)−N(1) = 99.19(14), and N(2)−Fe(1)−P(2) = 80.30(12)°). For the Fe(2) site, the sum of the angles in the basal plane, 353.17°, is close to 360° (N(6)−Fe(2)−N(3) = 122.29(14)°, N(6)−Fe(2)−P(4) = 105.16(13)°, and P(4)−Fe(2)−N(3) = 125.72(10)°). The average angle of the axial ligand from the basal plane is close to 90° (N(4)−Fe(2)−N(6) = 113.38(16), N(4)−Fe(2)−N(3) = 101.56(16), and N(4)−Fe(2)−P(4) = 79.96(10)°). The bond lengths of the ligands to the Fe(1) ion in the trigonal plane for [Fe(NpNP^{iPr})]$_2$(μ-N_2) are Fe(1)−N(1) = 1.983(4), Fe(1)−N(2) = 2.117(4), Fe(1)−

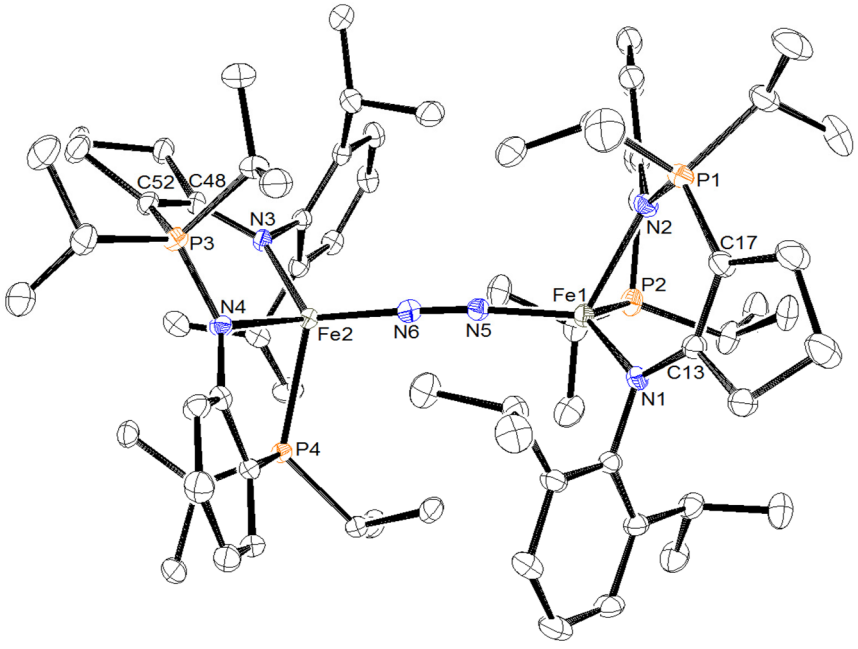

Figure 4. ORTEP drawing of the crystal structure of [Fe(NpNP^{iPr})]$_2$(μ-N_2) with ellipsoids at the 30% probability level. All hydrogen atoms have been omitted for clarity. Selected bond lengths (Å) and angles (deg): Fe(1)−P(2) 2.3486(16), N(5)−N(6) 1.186(6), Fe(1)−N(1) 1.983(4), Fe(1)−N(2) 2.117(4), Fe(1)−N(5) 1.800(4), Fe(2)−P(4) 2.3466(13), Fe(2)−N(3) 1.992(4), Fe(2)−N(4) 2.125(4), Fe(2)−N(6) 1.812(4), P(1)−N(2) 1.614(4), P(1)−C(17) 1.758(5), P(2)−C(29) 1.823(5), P(3)−N(4) 1.622(5), P(3)−C(52) 1.747(5), P(4)−C(64) 1.815(5), N(1)−C(13) 1.340(6), N(2)−C(24) 1.407(6), N(3)−C(48) 1.351(7), N(4)−C(59) 1.400(6), C(13)−C(17) 1.384(6), C(24)−C(29) 1.416(8), C(48)−C(52) 1.383(7), C(59)−C(64) 1.430(8).

DOI: 10.1021/acs.inorgchem.5b00536
Inorg. Chem. 2015, 54, 9271−9281

Table 1. Selected Bond Lengths and $\nu(N_2)$ Stretching Vibration Frequencies of $[Fe(NpNPiPr)_2]_2(\mu\text{-}N_2)$ and a Comparison with Bond Lengths and $\nu(N_2)$ Stretching Vibration Frequencies of Formally Monovalent Iron Dinitrogen Compounds Reported Previously

complex	coordination number	Fe−N (Å)	N−N (Å)	ν_{NN} (cm^{-1})	ref
$[Fe(nacnac^{Me})(tBupy)]_2(\mu\text{-}N_2)$	4	1.816(2)	1.151(3)	1770[a]	8d
$[Fe(nacnac^{tBu})(tBupy)]_2(\mu\text{-}N_2)$	4	1.804(2), 1.794(2)	1.161(4)		8d
$[Fe(NpNP^{iPr})]_2(\mu\text{-}N_2)$	4	1.800(4), 1.814(4)	1.184(6)	1755[a]	this work
$[Fe(nacnac^{Me})]_2(\mu\text{-}N_2)$	3	1.745(3), 1.775(2)	1.186(7), 1.172(5)	1810[a]	8d
$[Fe(nacnac^{tBu})]_2(\mu\text{-}N_2)$	3	1.760(6), 1.778(6)	1.182(5)	1778[a]	8d
$[Fe(PhBP^{iPr}_3)]_2(\mu\text{-}N_2)$	4	1.811(5), 1.818(5)	1.138(6)		16
$[Fe(SiP^{iPr}_3)(N_2)]$	5	1.817(4)	1.1065(5)	2008[b]	9c
$[Fe(SiP^{Ph}_3)(N_2)]$	5	1.819(2)	1.106(3)	2041[b]	17
$\{[(ArN)_2C^{tBu}]Fe\}_2(\mu\text{-}N_2)$	8	1.834(3)	1.124(6)	2005[a]	18
$\{Fe[N(SiMe_2N^{tBu})(C_2H_4PiPr_2)]\}_2(\mu\text{-}N_2)$	4	1.8510(15)	1.166(3)	1760[a]	19

[a]Measured by resonance Raman spectroscopy. [b]Measured by IR spectroscopy.

N(5) = 1.800(4), and Fe(1)−P(2) = 2.3486(16) Å, while those around Fe(2) are Fe(2)−N(3) = 1.992(4), Fe(2)−N(4) = 2.125(4), Fe(2)−N(6) = 1.814(4), and Fe(2)−P(4) = 2.3466(13) Å. The formally monovalent Fe(I)−dinitrogen bonds (Fe(1)−N(5) = 1.800(4) and Fe(2)−N(6) = 1.814(4) Å) are similar to those of $[Fe(nacnac^{Me})(tBupy)]_2(\mu\text{-}N_2)$ reported previously (Fe−N_2 = 1.800(4) and 1.814(4) Å).[8b,d] The N−N bond length of the bridged N_2 molecule in $[Fe(NpNP^{iPr})]_2(\mu\text{-}N_2)$ is N(5)−N(6) = 1.184(6) Å, which is significantly longer than that of metal-free N_2 (1.098 Å) and slightly elongated compared with those of mononuclear and dinuclear Fe(I) complexes bound with a dinitrogen molecule (Table 1).

The activated nature of dinitrogen was also clearly indicated by vibrational spectroscopy. The resonance Raman spectra of the dinitrogen complexes as measured with 532 nm excitation contain a band assignable to the $\nu(N_2)$ stretching vibration of μ-N_2 at 1755 cm^{-1} for $[Fe(NpNP^{iPr})]_2(\mu\text{-}N_2)$ that shifts to 1700 cm^{-1} when $^{15}N_2$ is employed instead of $^{14}N_2$ (Figure 5). The isotope shift is within the range of the shift expected for a coordinated dinitrogen molecule. The observed μ-N_2 is at a lower frequency than the analogous stretching vibrations of $[Fe(nacnac^{Me})(tBupy)]_2(\mu\text{-}N_2)$ (^{14}N 1770/^{15}N 1708 cm^{-1}) and $[Fe(nacnac^{tBu})]_2(\mu\text{-}N_2)$ (^{14}N 1778 cm^{-1}) reported by Holland and co-workers[8b,d] and has the lowest frequency value among those reported previously. This indicates that the N_2 molecule is moderately activated by a formally monovalent Fe(I) complex with an $NpNP^{iPr}$ ligand (Table 1).

The ^1H NMR spectrum of $[Fe(NpNP^{iPr})]_2(\mu\text{-}N_2)$ in C_6D_6 is broad and shifted, consistent with the presence of paramagnetic iron centers (Figure S6 in the Supporting Information); the solution-state magnetic moment of $\mu_{eff} = 6.91\mu_B$ (indicating six unpaired electrons) was measured by the Evans method.[15] In order to study the oxidation and spin states of the metal center, we measured the Mössbauer spectrum of the complex $[Fe(NpNP^{iPr})]_2(\mu\text{-}N_2)$. The spectrum at 78 K showed a quadrupole doublet with isomer shift (δ) of 0.73 mm/s and a quadrupole splitting (ΔE_Q) of 1.83 mm/s (Figure 6), which are similar to those of $[Fe(nacnac^{Me})]_2(\mu\text{-}N_2)$[8f] reported previously (δ = 0.62 mm/s, ΔE_Q = 1.41 mm/s). This indicates that one electron from each iron is transferred to an antibonding π^* orbital of the dinitrogen molecule by π back-donation, and the resultant transferred electron of dinitrogen is antiferromagnetically coupled with an unpaired electron of high-spin Fe(II) with four unpaired electrons; the spin state of $[Fe(NpNP^{iPr})]_2(\mu\text{-}N_2)$ is $S = 3$ with antiferromagnetic coupling between dianionic N_2^{2-} and diiron(II).

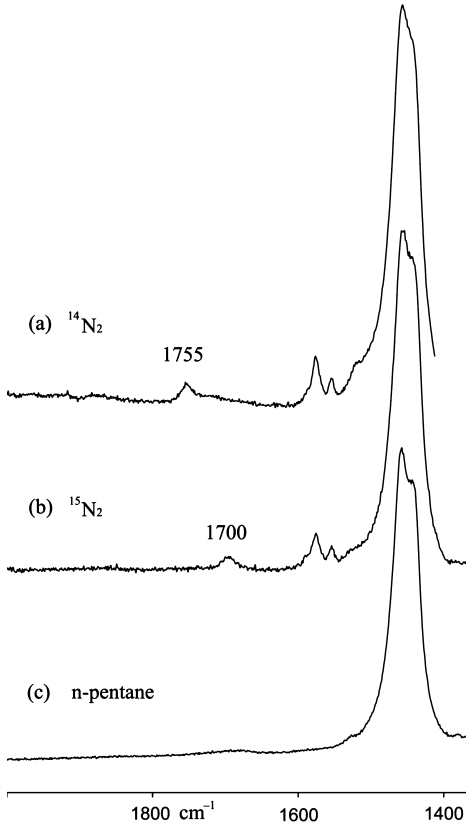

Figure 5. Resonance Raman spectra of $[Fe(NpNP^{iPr})]_2(\mu\text{-}N_2)$ in *n*-pentane: (a) $[Fe(NpNP^{iPr})]_2(\mu\text{-}^{14}N_2)$ in *n*-pentane, (b) $[Fe(NpNP^{iPr})]_2(\mu\text{-}^{15}N_2)$ in *n*-pentane, and (c) *n*-pentane.

DFT Calculations on $[Fe(NpNP^{iPr})]_2(\mu\text{-}N_2)$. The molecular structure optimized for $[Fe(NpNP^{iPr})]_2(\mu\text{-}N_2)$ in the $S = 3$ state was found to be essentially identical to the structure obtained by X-ray analysis within 0.08 Å, except for the Fe−P bonds. Such longer bonds are often seen in the structures optimized under vacuum conditions. The calculated frequency of the $\nu(N_2)$ stretching vibration, 1753 cm^{-1}, also agrees well with that obtained by Raman measurement. The electronic structure of the dinitrogen diiron complex was assessed using density functional theory (DFT) calculation results obtained on the basis of the crystal structure of $[Fe(NpNP^{iPr})]_2(\mu\text{-}N_2)$.

DOI: 10.1021/acs.inorgchem.5b00536
Inorg. Chem. 2015, 54, 9271−9281

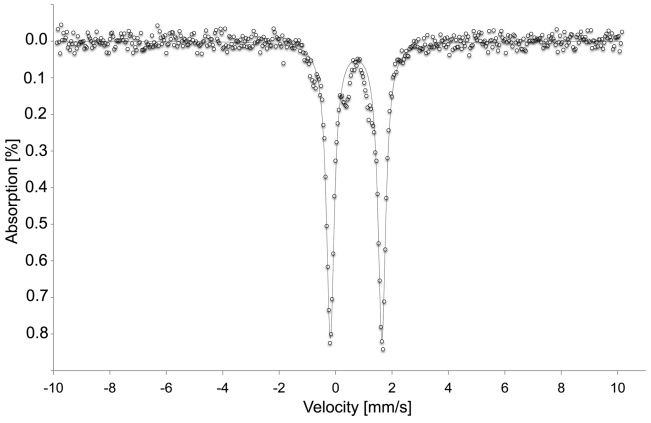

Figure 6. Zero-field ^{57}Fe Mössbauer spectrum of $[Fe(NpNP^{iPr})]_2(\mu\text{-}N_2)$ at 78 K. The dotted line shows the experimental data, and the solid line is the fitted curve using the parameters δ = 0.73 mm/s and ΔE_Q = 1.83 mm/s. The line width at half-maximum of the Lorentzian peaks was estimated to be 0.34 mm/s. The small unfitted areas seen in the figure are probably due to impurities.

The differential density and spin density maps are shown in Figure 7a,b, respectively. The density increases in the vicinity of

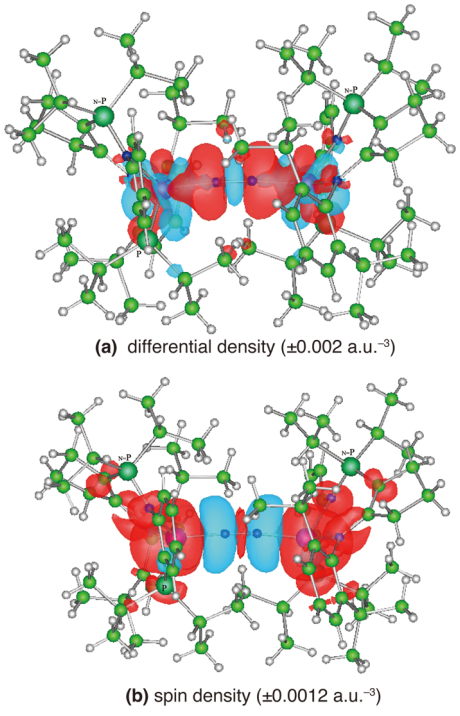

Figure 7. (a) Differential density map with respect to dinitrogen complexation in $[Fe(NpNP^{iPr})]_2(\mu\text{-}N_2)$. The red and blue regions indicate increases and decreases in electron density, respectively, that occur upon complexation. (b) Spin density map of $[Fe(NpNP^{iPr})]_2(\mu\text{-}N_2)$. The red and blue regions show excess densities of α spin and β spin, respectively.

the Fe−N bond axes and considerably decreases in the N−N σ-bonding and lone-pair orbitals. The differential density map can be interpreted using the spin density map (Figure 7b). The increase in the electron density seen in the vicinity of the coordinated dinitrogen molecule is induced by β-spin density. That is, the decrease in the electron density in the N−N bonding region is due to σ donation from the dinitrogen to the metal as well as π back-donation from the metal to the dinitrogen, which weakens the N−N bond of the dinitrogen molecule. Interestingly, no differences were observed in the electron density around the chelating ligand upon coordination of dinitrogen to the iron sites, as shown in Figure 7a. This indicates that the negative charge on the $NpNP^{iPr}$ ligand functions as a barrier to electron back-flow to assist the π back-donation from the iron center to the dinitrogen ligand. The change in the electron distribution at the phosphine ligand is attributed to a change in electron configuration between the two dπ orbitals on each iron center that are hyperconjugated with the P−C σ* orbital. This suggests that some amount of electron density on the iron center pushed out by σ donation from the phosphine ligands is moved into the P−C σ* orbital, which might be similar to the case of $[Fe(PhBP^{iPr}_3)]_2(\mu\text{-}N_2)$.[16]

On the basis of the results of natural population analysis for $[Fe(NpNP^{iPr})]_2(\mu\text{-}N_2)$ (Table 2), increases in negative charge and β-spin density on the dinitrogen ligand were also observed. The spin density on the iron center was found to be 3.28 and the atomic charge of dinitrogen was found to be −0.70, indicating that the electron density transferred from the high-spin Fe(I) centers to the dinitrogen ligand is less than 1. For comparison, we also carried out DFT calculations on the diiron dinitrogen complexes with β-diketiminato ligands reported previously by Holland et al., namely, $[Fe(nacnac^{Me})]_2(\mu\text{-}N_2)$, $[Fe(nacnac^{Me})(tBupy)]_2(\mu\text{-}N_2)$, and $[Fe(nacnac^{tBu})(tBupy)]_2(\mu\text{-}N_2)$.[8d] The atomic charges and spin densities of these complexes are listed together in Table 2. The infusion of electron density into dinitrogen increases in the following order: $[Fe(nacnac^{Me})(tBupy)]_2(\mu\text{-}N_2)$ < $[Fe(nacnac^{tBu})(tBupy)]_2(\mu\text{-}N_2)$ < $[Fe(NpNP^{iPr})]_2(\mu\text{-}N_2)$ < $[Fe(nacnac^{Me})]_2(\mu\text{-}N_2)$. This appears to be due to the presence of a larger negative charge (−1.10, −1.09) on the phosphoranimine N atom for $[Fe(NpNP^{iPr})]_2(\mu\text{-}N_2)$ than on the nacnac N atoms of the reference complexes with the same coordination number, $[Fe(nacnac^{Me})]_2(\mu\text{-}N_2)$ (−0.69, −0.69), $[Fe(nacnac^{Me})(tBupy)]_2(\mu\text{-}N_2)$ (−0.65, −0.65), and $[Fe(nacnac^{tBu})(tBupy)]_2(\mu\text{-}N_2)$ (−0.65, −0.69). The larger negative charge may have contributed to an increase in π back-donation from the metal to the dinitrogen. The charges on the metal centers in $[Fe(NpNP^{iPr})]_2(\mu\text{-}N_2)$ (0.73, 0.72) are less than those of the reference complexes, $[Fe(nacnac^{Me})]_2(\mu\text{-}N_2)$ (0.93, 0.93), $[Fe(nacnac^{Me})(tBupy)]_2(\mu\text{-}N_2)$ (0.95, 0.95) and $[Fe(nacnac^{tBu})(tBupy)]_2(\mu\text{-}N_2)$ (0.97, 0.97). This suggests that the electron density on the iron centers is due to σ donation from the phosphine ligands, which promotes the π back-donation from the metal to the dinitrogen.

Orbital Overlap Interactions between the Coordinated Dinitrogen and the Iron Metal Center. To discuss the contribution of the $NpNP^{iPr}$ ligand to activation of the coordinated dinitrogen, we focused on the four highest occupied β orbitals (Figure S7 in the Supporting Information), which are the most important orbitals when we consider the bonding nature. Interestingly, these orbitals are all involved in π back-donation from the iron centers to dinitrogen. The electron distribution on dinitrogen in the upper two orbitals is at least two-thirds as large as that on the iron centers (as shown by the percentage of components of atomic orbitals described in Figure S7a,b). This observation provides insights into the formal iron(I) ion, which includes iron(II) ion character. Additionally, hyperconjugation was identified between the phosphine σ*(P−C) orbital and the metal dδ orbitals with the nodal plane along the Fe−P bond. This leads to a modest

DOI: 10.1021/acs.inorgchem.5b00536
Inorg. Chem. 2015, 54, 9271−9281

Table 2. Population Analysis for Diiron μ-Dinitrogen Complexes

	$[Fe(NpNP^{iPr})]_2(\mu\text{-}N_2)$		$[Fe(nacnac^{Me})]_2(\mu\text{-}N_2)^a$		$[Fe(nacnac^{Me})(t\text{Bupy})]_2(\mu\text{-}N_2)^a$		$[Fe(nacnac^{tBu})(t\text{Bupy})]_2(\mu\text{-}N_2)^a$	
bond lengths (Å)								
N−N	1.186		1.185		1.151		1.167	
Fe−N	1.799	1.812	1.746		1.815		1.800	1.799
planarity[b]	337.7	337.2	359.1	359.1	345.6	345.6	349.0	350.4
atomic charges								
N_2[c]	−0.70		−0.77		−0.65		−0.69	
Fe	0.73	0.72	0.93	0.93	0.95	0.95	0.97	0.97
N(diket)[d]	−0.72	−0.73	−0.69	−0.69	−0.69	−0.69	−0.70	−0.65
N(imino/diket)[e]	−1.10	−1.09	−0.69	−0.69	−0.65	−0.65	−0.65	−0.69
atomic spin density								
Fe	3.28		3.30		3.37		3.37	
N_2[c]	−0.83		−0.91		−0.79		−0.82	
orbital overlap population between Fe and N								
MO[f]	0.100	0.099	0.101	0.101	0.092	0.092	0.095	0.095
NO[g]	0.141	0.136	0.146	0.146	0.126	0.126	0.130	0.130

[a]The crystal structure was taken from ref 8d. [b]The sum of the three angles around an iron center with respect to the chelate ring and the dinitrogen ligand, as a measure of coplanarity. The value 360° indicates that the dinitrogen ligand is completely coplanar with the chelate ring. [c]The total charge/spin density of the dinitrogen ligand. [d]The N atoms attached to a phenyl group in our complex, one pair of N atoms in each β-diketiminate ligand furthest apart in complex $[Fe(nacnac^{Me})(t\text{Bupy})]_2(\mu\text{-}N_2)$, and the pair of N atoms furthest apart from the pyridine attached to the other center in complex $[Fe(nacnac^{tBu})(t\text{Bupy})]_2(\mu\text{-}N_2)$. [e]The imino N atom in our complex and the other pair of N atoms in each β-diketiminate ligand in complex $[Fe(nacnac^{Me})(t\text{Bupy})]_2(\mu\text{-}N_2)$ and $[Fe(nacnac^{tBu})(t\text{Bupy})]_2(\mu\text{-}N_2)$. [f]The sum of $Q_{i,Fe-N}$ for the four highest occupied Kohn−Sham β orbitals. [g]The sum of $Q_{i,Fe-N}$ for the natural orbitals having π bonding and antibonding nature between iron and dinitrogen.

lowering of the dδ orbital energy (Figure S7c,d), as described in Chart 1. On the other hand, in $[Fe(nacnac^{Me})(t\text{Bupy})]_2(\mu\text{-}N_2)$,[8d] such hyperconjugation between the $nacnac^{Me}$ ligand and the dδ orbitals of the metal ion has not been found (Chart S1 in the Supporting Information).

The orbital overlap interactions between metal d orbitals and dinitrogen orbitals were evaluated by examining the $Q_{Fe-N}(MO)$ values (eq 5 in the Experimental Section), which are listed in Table 2. Interestingly, the $Q_{Fe-N}(MO)$ values for $[Fe(NpNP^{iPr})]_2(\mu\text{-}N_2)$ (0.100, 0.099) are larger than those of $[Fe(nacnac^{Me})(t\text{Bupy})]_2(\mu\text{-}N_2)$ (0.092, 0.092) and $[Fe(nacnac^{tBu})(t\text{Bupy})]_2(\mu\text{-}N_2)$ (0.095, 0.095), although their Fe−N bond lengths are almost the same within experimental error. Also, the values for $[Fe(NpNP^{iPr})]_2(\mu\text{-}N_2)$ are similar to those for $[Fe(nacnac^{Me})]_2(\mu\text{-}N_2)$ (0.101, 0.101), although the Fe−N bonds of the former are longer than those of the latter. These findings indicate that the infusion of electrons into the dinitrogen molecule depends on the orbital overlap interaction rather than the Fe−N bond lengths.

We considered the orbital overlap of the dπ orbitals with the dinitrogen π^* orbitals in the series of diiron dinitrogen nacnac complexes $[Fe(nacnac^{Me})]_2(\mu\text{-}N_2)$, $[Fe(nacnac^{Me})(t\text{Bupy})]_2(\mu\text{-}N_2)$, and $[Fe(nacnac^{tBu})(t\text{Bupy})]_2(\mu\text{-}N_2)$ to compare with that in $[Fe(NpNP^{iPr})]_2(\mu\text{-}N_2)$. In $[Fe(nacnac^{Me})]_2(\mu\text{-}N_2)$, the effective orbital overlap of the dπ orbitals with the dinitrogen π^* orbitals, which are essentially coplanar with both of the iron−nacnac planes (359.1°, 359.1°), results in substantial electron donation from the metal to the dinitrogen. On the other hand, the orbital overlaps of the dπ orbitals with the dinitrogen π^* orbitals in $[Fe(nacnac^{Me})(t\text{Bupy})]_2(\mu\text{-}N_2)$ and $[Fe(nacnac^{tBu})(t\text{Bupy})]_2(\mu\text{-}N_2)$ are less than that in $[Fe(nacnac^{Me})]_2(\mu\text{-}N_2)$. This is explained in terms of the fact that the iron−nacnac planes of the former two complexes are bent out of the nodal plane of one dinitrogen π^* orbital (345.6°, 345.6° for $[Fe(nacnac^{Me})(t\text{Bupy})]_2(\mu\text{-}N_2)$ and 349.0°, 350.4° for $[Fe(nacnac^{tBu})(t\text{Bupy})]_2(\mu\text{-}N_2)$) in comparison with that of the latter, as shown in Table 2. In $[Fe(NpNP^{iPr})]_2(\mu$-

Chart 1. Orbital Interactions between the dπ and dδ Orbitals of Fe and the π^* Orbitals of the Coordinated Dinitrogen Using Virtual Coordination Structures for $[Fe(NpNP^{iPr})]_2(\mu\text{-}N_2)$[a]

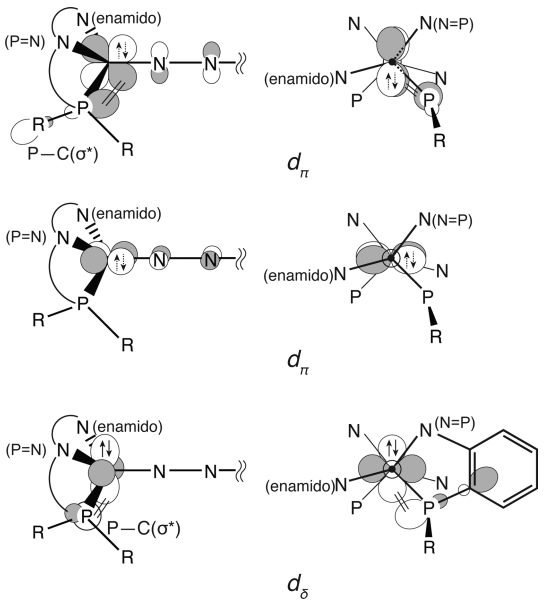

[a](top, bottom) Hyperconjugation of (top) a dπ orbital and (bottom) a dδ orbital on each iron center with the σ^*(P−C) orbital of the coordinated phosphine ligand controls the orientations of the dπ orbitals, leading to a great orbital overlap between the iron dπ orbital and a π^* orbital of the coordinated dinitrogen. The donor−acceptor interaction energies evaluated with second-order perturbation theory based on NBO are listed in Table S2 in the Supporting Information. Stabilization energies arising from the donor−acceptor interaction are (top) 0.98 to 1.06 and (bottom) 1.46 to 1.61 kcal/mol. (middle) Hyperconjugation between Fe and the $NpNP^{iPr}$ ligand is not observed.

DOI: 10.1021/acs.inorgchem.5b00536
Inorg. Chem. 2015, 54, 9271−9281

N_2), the electron infusion into the dinitrogen is as large as that in $[Fe(nacnac^{Me})]_2(\mu\text{-}N_2)$ in spite of a large deviation of the π^* orbitals from the enamido−iminophosphorane N−P−N plane (337.7°, 337.2°). The orbital overlaps of the iron dπ orbitals with the dinitrogen π^* orbitals, as described above, are induced by hyperconjugation (Chart 1 top and bottom): the σ^*(P−C(isopropyl)) orbital of the coordinated phosphine ligand overlaps attractively with one of the two dπ orbitals on each iron center (Chart 1 top), and the σ^*(P−C(phenyl)) orbital of the same phosphine ligand overlaps attractively with the dδ orbitals (Chart 1 bottom). The orientations of the dπ orbitals on the iron center are controlled by the hyperconjugation with the phosphine ligand and by the negative charge on the N atoms of the $NpNP^{iPr}$ ligand; both of these N atoms are just placed on the nodal planes of a dπ orbital. As structural evidence, the dihedral angles between the plane defined by the Fe, P, and dinitrogen N atoms and the plane defined by the Fe, N(phosphoranimine), and dinitrogen N atoms (86.2° and 85.4°, respectively) are close to a right angle. Furthermore, the P−Fe−N(N_2) bond angles are 104.55(13)° and 105.16(13)°, which are close to a right angle in comparison with the corresponding angles of N(enamido)−Fe−N(N_2) (122.33(16)°, 122.29(14)°) and N(iminophosphorane)−Fe−N(N_2) (116.23(17)°, 113.38(16)°).

Therefore, the dinitrogen molecule in $[Fe(NpNP^{iPr})]_2(\mu\text{-}N_2)$ is moderately activated by the supporting functional $NpNP^{iPr}$ ligand in spite of the bending of the nodal plane of one dinitrogen π^* orbital from the enamido−iminophosphorane N−P−N plane. This indicates that dinitrogen activation is promoted by a strong interaction between the phosphine ligand and the Fe dδ/dπ orbitals. Additionally, as described above, it is very important that the significant activation of the coordinated dinitrogen molecule is also induced by the greater negative charge on the iminophosphorane groups. We can propose that the combination of the phosphine and iminophosphorane groups of the functional $NpNP^{iPr}$ ligand system provide activation of the dinitrogen molecule.

CONCLUSION

We have succeeded in synthesizing $[Fe(NpNP^{iPr})]_2(\mu\text{-}N_2)$, a novel diiron dinitrogen complex, using our new $NpNP^{iPr}$ ligand, which includes an iminophosphorane backbone with strong σ-donating ability. The crystal structure of $[Fe(NpNP^{iPr})]_2(\mu\text{-}N_2)$ revealed a formally monovalent diiron(I) complex bridged by a dinitrogen molecule. The two iron sites are twisted around the dinitrogen molecule with a torsion angle of 92.07°. The N−N bond length of 1.184(6) Å is very close to the N−N bond lengths of the previously reported diiron dinitrogen complexes $[Fe(nacnac^{tBu})]_2(\mu\text{-}N_2)$ (1.182(5) Å) and $[Fe(nacnac^{Me})]_2(\mu\text{-}N_2)$ (1.186(7) Å). The N−N bond in $[Fe(NpNP^{iPr})]_2(\mu\text{-}N_2)$ lies in the longest bond range among those of diiron(I) dinitrogen complexes reported previously.[8d] The $\nu(^{14}N_2/^{15}N_2)$ stretching vibration frequencies, 1755/1700 cm^{-1}, are the lowest frequencies observed among the formally monovalent diiron(I) dinitrogen complexes reported previously (Table 1). The Mössbauer spectrum at 78 K showed a quadrupole doublet with δ = 0.73 mm/s and ΔE_Q = 1.83 mm/s. The diiron dinitrogen complex is paramagnetic in benzene solution (S = 3, μ_{eff} = 6.91μ_B) and can be considered to contain two iron(II) ions, each in the high-spin d^6 state. The two Fe(II) ions (S = 2 for each) and N_2^{2-} are antiferromagnetically coupled, similar to the case of $[Fe(nacnac^{Me})]_2(\mu\text{-}N_2)$. DFT calculations provided evidence that the electronic state of the coordinated dinitrogen molecule is N_2^{2-}. The effective activation of dinitrogen through π back-donation is induced by the $NpNP^{iPr}$ ligand system, which has negative charges on the enamido N and phosphoranimine N atoms and the strong electron-donating ability of the phosphine.

EXPERIMENTAL SECTION

Caution! *Because of the sensitivity of the n-BuLi and KC_8 reagents toward moisture and oxygen, these should be handled with great care.*

General Methods. All manipulations were carried out under an atmosphere of purified argon or dinitrogen gas in an MBRAUN MB 150B-G glovebox or by standard Schlenk techniques. ^1H and ^{31}P NMR spectra were measured on a Varian Mercury 300 spectrometer, and ^1H and ^{31}P chemical shifts were estimated relative to TMS and H_3PO_4 as internal standards, respectively. Fourier transform infrared (FT-IR) spectra of solid compounds were measured on KBr pellets using a JASCO FT/IR-410 spectrophotometer. Elemental analyses were obtained with a PerkinElmer CHN-900 elemental analyzer. Magnetic moment measurements (Evans method) in the solid state were obtained using a Sherwood Scientific Ltd. MSB-MKI magnetic susceptibility balance. The solution-state magnetic moments were determined by the Evans method using ^1H NMR spectroscopy.[15] Resonance Raman spectral measurements were carried out using a JASCO NKS-1000 spectrophotometer. Raman scattering was excited using the 532 nm emission from an Ar laser (Laser Quantum, Ventus 532) and detected using a CCD detector (Andor, DU420-OE) attached to a single polychromator (Ritsu Oyo Kogaku, DG-1000). Spectra were recorded at ambient temperature, and the laser power at the sample point was 30 mW. The slit width was set to 200 μm. All measurements were carried out with samples contained in a spinning cell (3000 rpm) at room temperature. Raman shifts were calibrated with indene, and the accuracy of the peak positions of the Raman bands was ±1 cm^{-1}.

Zero-field ^{57}Fe Mössbauer spectra were recorded on a spectrometer (Topologic Systems Inc.) at 78 K in constant-acceleration mode. $^{57}Co/Rh$ was used as the radiation source. MossWinn 4.0Pre software (http://www.mosswinn.com/) was used for quantitative evaluation of the spectral parameters (least-squares fitting to Lorentzian peaks). Isomer shifts were determined relative to α-iron at 298 K.

The τ value is defined in terms of the difference between the sum of the basal ligand−basal ligand angles and the sum of the basal ligand−axial ligand angles:[13]

$$\tau = \frac{\sum(\text{basal−M−basal}) - \sum(\text{basal−M−axial})}{90^\circ} \quad (1)$$

X-ray Crystallography. All of the single crystals obtained ($HNpNP^{iPr}$, $Li(NpNP^{iPr})$, $FeBr(NpNP^{iPr})$, and $[Fe(NpNP^{iPr})]_2(\mu\text{-}N_2)$) were analyzed by X-ray diffraction. Each crystal was mounted on a glass fiber, and diffraction data were collected using a Rigaku/MSC Mercury CCD with graphite-monochromatized Mo Kα radiation at −100 or −150 °C. All crystal data and experimental details are listed in Table S1 in the Supporting Information. The crystal structures were solved by a combination of direct methods (SIR92[20]) and Fourier techniques. All non-hydrogen atoms were refined anisotropically. Hydrogen atoms were refined by the riding model using the appropriate HFIX command in SHELXL97.[21] The Sheldrick weighting scheme was applied for all crystals. Plots of $\sum(|F_o| - |F_c|)^2$ versus $|F_0|$, reflection order in data collection, sin θ/λ, and various classes of indices showed no unusual trends. Neutral atomic scattering factors were taken from Cromer and Waber.[22] Anomalous dispersion effects were included in F_{calc},[23] and the values for $\Delta f'$ and $\Delta f''$ were obtained from Creagh and McAuley.[24] The values for the mass attenuation coefficients are those of Creagh and Hubbell.[25] All of the calculations were performed using the CrystalStructure crystallographic software package.

General Procedures. All of the reagents employed were commercially available. Toluene, THF, and diethyl ether were purchased in anhydrous form from Wako Ltd. and passed through

DOI: 10.1021/acs.inorgchem.5b00536
Inorg. Chem. 2015, 54, 9271−9281

columns containing activated alumina and Ridox catalyst. C_6D_6 was dried by distillation from sodium/benzophenone. Diisopropylamine was dried over CaH_2 and distilled prior to use. *n*-Butyllithium was purchased from Aldrich, and the concentration was determined via direct titration with diphenylcarboxylic acid. KC_8 was prepared according to a literature procedure.[26] All other compounds were purchased from commercial suppliers and used as received. 2,6-Diisopropyl-*N*-(2-diisopropylphosphinocyclopentylidene)aniline (HNP^{iPr}) was synthesized according to the previously published method.[11] *o*-Bromophenyl azide was prepared as outlined below.[27]

DFT Calculation Details. The most stable structure of the diiron dinitrogen complex obtained in the present work was determined by a full optimization of the structure using a DFT calculation in which the crystal structure obtained by X-ray analysis was employed as the starting complex. The DFT calculations for electron and spin density analyses were performed using the crystal structure of $[Fe(NpNP^{iPr})]_2(\mu\text{-}N_2)$ for the sake of comparison with other compounds. The calculations were carried out using the B3LYP functional.[28] The following basis sets were used for the respective atoms: 6-311G(d) for Fe,[29a,b] P,[29c] N, and olefin C of the chelate ring[29d] and 6-31G(d)[29e,f] for other C and H atoms. For drawing electron density maps, 6-311G was employed for the Fe atom. Two diffuse p functions, which were developed by Wachters, were added to the basis set of the Fe atom. These functions were multiplied by 1.5.[29a] For the spin state of the Fe atom, $S = 3$, which was obtained from magnetic moment with Evans method, was employed for $[Fe(NpNP^{iPr})]_2(\mu\text{-}N_2)$.

In order to examine the change in electron density accompanying coordination of a dinitrogen molecule to a pair of the corresponding monoiron complexes, a differential density function, $\Delta\rho(\mathbf{r})$, was evaluated according to eq 2:

$$\Delta\rho(\mathbf{r}) = \rho(\mathbf{r}, \text{ diiron dinitrogen complex}) - \{\rho(\mathbf{r}, \text{ diiron complex without dinitrogen}) + \rho(\mathbf{r}, \text{ dinitrogen})\} \quad (2)$$

where $\rho(\mathbf{r}, X)$ on the right represents electron density at a point $\mathbf{r}$ for species X with atomic coordinates in the crystal structure of the diiron dinitrogen complex.

The quantitative changes in natural atomic charges and spin densities that occur upon coordination of dinitrogen to the metal complexes were estimated.[30] Mulliken population analysis[31] was carried out for the four highest occupied Kohn–Sham β orbitals concerning the π back-donation from iron to dinitrogen, and the orbital overlap populations ($Q_{i,Fe-N}$; eq 3) and gross populations ($q_{i,Fe}$ and $q_{i,N}$; eq 4) were calculated in order to evaluate the contributions to the interaction between the iron ions and dinitrogen and their compositions:

$$Q_{i,Fe-N} = \sum_{a\in Fe}\sum_{b\in N} C_{ai}C_{bi}S_{ab} \quad (3)$$

$$q_{i,A} = \sum_{a\in A}\sum_{b\in all} C_{ai}C_{bi}S_{ab} \quad (4)$$

where A denotes Fe or dinitrogen N, S_{ab} is the overlap integral between atomic orbitals a and b, and $C_{\mu i}$ is the molecular orbital coefficient for atomic orbital μ in the ith molecular orbital. The sum of $Q_{i,Fe-N}$ for the four orbitals ($Q_{Fe-N}(MO)$; eq 5) was estimated as a measure of π back-donation from the metal dπ orbitals to the dinitrogen π^* orbitals. The sum of $Q_{i,Fe-N}$ weighted by the occupation number n_i for the natural orbitals ($Q_{Fe-N}(NO)$; eq 5) was also estimated as a measure of the overlap contributed by both the α and β electrons, where the contributions of π-bonding and π-antibonding character between iron and dinitrogen predominate in comparison with the Kohn–Sham orbitals.

$$Q_{Fe-N}(MO/NO) = \sum_i n_i \sum_{a\in Fe}\sum_{b\in N} C_{ai}C_{bi}S_{ab} \quad (5)$$

where $n_i = 1$ for occupied Kohn–Sham β orbitals.

For comparison, a similar analysis was carried out for three diiron dinitrogen complexes with low-coordinate β-diketiminato derivatives reported previously by Holland et al.:[8d] $[Fe(nacnac^{Me})]_2(\mu\text{-}N_2)$ (three-coordinate), $[Fe(nacnac^{Me})(tBupy)]_2(\mu\text{-}N_2)$ (two-coordinate), and $[Fe(nacnac^{tBu})(tBupy)]_2(\mu\text{-}N_2)$ (two-coordinate). The π back-bonding interaction with the σ^* orbital along the P–C bond was evaluated with second-order perturbation theory analysis of the Fock matrix in the NBO basis.[32]

All of the electronic structure calculations were performed using Gaussian 09, revision D.01,[33] and the isosurfaces of the molecular orbitals were drawn using the MOPLOT and MOVIEW programs[34] on the Fujitsu CX400 system at the Nagoya University Information Technology Center.

Preparation of $LiNpNP^{iPr}$ and $HNpNP^{iPr}$. *Synthesis of o-Bromophenyl Azide (2-Br-Ar-N_3).* The compound was prepared by a modification of a literature procedure.[27] *o*-Bromoaniline (6.4 g, 37.2 mmol) was added to 5 mL of concentrated hydrochloric acid and 30 mL of water in an ice bath. To the cold solution was slowly added 20 mL of an aqueous solution of $NaNO_2$ (2.57 g, 37.2 mmol), and the resulting mixture was stirred at 0 °C for 0.5 h. This is an exothermic reaction, and the resulting diazonium salt is unstable at high temperatures. Stirring vigorously and keeping the temperature low is important. Excess nitrous acid was removed by addition of urea. NaN_3 (2.40 g, 37.2 mmol) was then added slowly to the reaction solution, and the resulting mixture was stirred for 1 h to obtain a white precipitate, which was extracted from the solution with 3 × 50 mL of diethyl ether. The combined extracts were washed with water and dilute hydrochloric acid (0.1 M) and dried over magnesium sulfate. The solvent was removed in vacuo, and the oily residue was isolated by silica gel chromatography with *n*-hexane as the eluent to yield the product as a pale-yellow oil (6.49 g, 32.7 mmol, 88% yield). ^{1}H NMR (300 MHz, δ/ppm in $CDCl_3$): 7.01 (t, 1H, Ar–H), 7.17 (d, 1H, Ar–H), 7.35 (t, 1H, Ar–H), 7.55 (d, 1H, Ar–H). FT-IR (ν/cm^{-1}): 2131, 2037 (azide).

Synthesis of (E)-N-(2-(((2-Bromophenyl)triazenylidene)-diisopropylphosphoranyl)cyclopentenyl)-2,6-diisopropylaniline ($HNpN_3Br^{iPr}$). Under a dinitrogen atmosphere, *o*-bromophenyl azide (16.5 g, 83.4 mmol) was added to a 10 mL solution of 2,6-diisopropyl-*N*-(2-diisopropylphosphinocyclopentylidene)aniline (HNP^{iPr}) in THF (30.0 g, 83.4 mmol). The resulting mixture was stirred at room temperature for 3 h. Volatiles were removed in vacuo. The desired compound was obtained as a yellow powder (41.5 g, 74.4 mmol, 89% yield). ^{1}H NMR (300 MHz, δ/ppm in benzene-d_6): 1.02–1.09, 1.19–1.31 (m, 24H, $(CH_3)_2CH$–Ar and $(CH_3)_2CH$–P), 1.59 (m, 2H, $CH_2CH_2CH_2$), 2.12 (m, 2H, $CH_2CH_2CH_2$), 2.23 (m, 2H, $CH_2CH_2CH_2$), 2.25 (m, 2H, $(CH_3)_2CH$–P), 3.45 (m, 2H, $(CH_3)_2CH$–Ar), 6.70–6.75 (m, 2H, Ar–H), 7.08–7.23 (m, overlapped, Ar–H), 7.61 (d, 1H, Ar–H), 7.73 (d, 1H, Ar–H) 10.53 (s, 1H, NH). ^{31}P NMR (121 MHz, δ/ppm in benzene-d_6): 50.18 (s). Anal. Calcd for $C_{29}H_{42}N_4P$: C, 62.47; H, 7.59; N, 10.05. Found: C, 62.35; H, 7.92; N, 9.98.

Synthesis of N-(2-Bromophenyl)-P,P-diisopropyl-P-(2-(2,6-diisopropylphenylamino)cyclopent-1-enyl)phosphoranimine ($HNpNBr^{iPr}$). Under a dinitrogen atmosphere, $HNpN_3Br^{iPr}$ (25 g, 44.8 mmol) was dissolved in toluene (100 mL) and heated at 80 °C for 1 day. The solvent was removed in vacuo. The resulting mixture was redissolved in *n*-pentane and stored at −35 °C. The desired compound was obtained as colorless crystals (17.5 g, 33.0 mmol, 74% yield). ^{1}H NMR (300 MHz, δ/ppm in benzene-d_6): 1.20–1.31 (m, 24H, $(CH_3)_2CH$–Ar and $(CH_3)_2CH$–P), 1.440 (m, 2H, $CH_2CH_2CH_2$), 1.85 (m, 2H, $CH_2CH_2CH_2$), 1.94 (m, 2H, $CH_2CH_2CH_2$), 2.32 (m, 2H, $(CH_3)_2CH$–P), 3.61 (m, 2H, $(CH_3)_2CH$–Ar), 6.54 (m, 1H, Ar–H), 7.08–7.14 (m, 3H, Ar–H, Ar–H), 7.21–7.25 (m, 2H, Ar–H, Ar–H), 7.67 (m, 1H, Ar–H) 10.99 (s, 1H, NH). ^{31}P NMR (121 MHz, δ/ppm in benzene-d_6): 34.98 (s).

Synthesis of N-(2-Diisopropylphosphinophenyl)-P,P-diisopropyl-P-(2-(2,6-diisopropylphenylamido)cyclopent-1-enyl)-phosphoranimine Lithium Salt ($LiNpNP^{iPr}$). Under a dinitrogen atmosphere, to a solution of *N*-(2-bromophenyl)-*P*,*P*-diisopropyl-*P*-(2-(2,6-diisopropylphenylamino)cyclopent-1-enyl)phosphoranimine in

DOI: 10.1021/acs.inorgchem.5b00536
Inorg. Chem. 2015, 54, 9271–9281

Et_2O (20 g, 37.7 mmol) was added *n*-BuLi (1.6 M, 47.2 mL, 75.5 mmol) dropwise at −78 °C. The resulting mixture was stirred for 4 h as it was warmed to 23 °C. The mixture was cooled to −78 °C again, and 20 mL of a diethyl ether solution of chlorodiisopropylphosphine (6 mL, 37.7 mmol) was added dropwise. Thereafter, the reaction mixture was warmed to ambient temperature overnight. Volatiles were removed in vacuo, and *n*-pentane was added to the mixture, which was then filtered through Celite using a glass frit. Excess *n*-pentane was removed in vacuo to give a dark-brown oil. The oil was dissolved in *n*-pentane again and stored in the freezer at −35 °C. The desired compound was obtained as a white powder (15.2 g, 26.5 mmol, 70% yield). Several recrystallizations of $LiNpNP^{iPr}$ from *n*-pentane gave colorless single crystals suitable for X-ray analysis. ^1H NMR (300 MHz, δ/ppm in benzene-d_6): 0.81−1.42 (m, 36H, $(CH_3)_2CH$−Ar and $(CH_3)_2CH$−P), 1.78 (m, 7 Hz, 2H, $CH_2CH_2CH_2$), 1.89 (m, 2H, $(CH_3)_2CH$−P), 2.32 (m, 2H, $CH_2CH_2CH_2$), 2.49−2.61 (m, 4H, $CH_2CH_2CH_2$ and $(CH_3)_2CH$−P), 3.63 (m, 7 Hz, 2H, $(CH_3)_2CH$−Ar), 6.74 (t, 1H, Ar−H), 6.92 (m, 1H, Ar−H), 7.09 (m, 1H, Ar−H), 7.15−7.21 (overlapped, Ar−H), 7.27 (d, 2H, Ar−H). ^{31}P NMR (121 MHz, δ/ppm in benzene-d_6): 38.78 (s), −6.68 (s). Anal. Calcd for $C_{35}H_{55}N_2P_2Li$: C, 73.40; H, 9.68; N, 4.89. Found: C, 73.17; H, 9.57; N, 4.82.

Synthesis of N-(2-Diisopropylphosphinophenyl)-P,P-diisopropyl-P-(2-(2,6-diisopropylphenylamino)cyclopent-1-enyl)-phosphoranimine ($HNpNP^{iPr}$). Under a dinitrogen atmosphere, Me_3NHCl (165 mg, 1.75 mmol) was added to 2 mL of a solution of $LiNpNP^{iPr}$ in THF (1 g, 1.75 mmol). The mixture was stirred at room temperature for 6 h. The reaction mixture was filtered to give a yellow solution. Volatiles were removed in vacuo, and 2 mL of *n*-pentane was added to the mixture, which was then stored in the freezer at −35 °C. The compound $HNpNP^{iPr}$ was obtained as a white powder (545 mg, 55% yield). Several recrystallizations of $HNpNP^{iPr}$ from *n*-pentane gave colorless single crystals suitable for X-ray analysis. ^1H NMR (300 MHz, δ/ppm in benzene-d_6): 0.97−1.13 (m, 12H, $(CH_3)_2CH$−P), 1.12−1.25 (m, 24H, $(CH_3)_2CH$−P and $(CH_3)_2CH$−Ar), 1.55 (m, 2H, $CH_2CH_2CH_2$), 2.06 (m, 2H, $CH_2CH_2CH_2$), 2.17−2.27 (m, 4H, $CH_2CH_2CH_2$ and $(CH_3)_2CH$−P), 3.32 (sep, 7 Hz, 2H, $(CH_3)_2CH$−Ar), 6.81 (t, 1H, Ar−H), 6.88 (m, 1H, Ar−H), 7.07 (d, 1H, Ar−H), 7.19 (overlapped, Ar−H), 7.21 (m, 2H, Ar−H), 9.00 (s, 1H, NH). $^{31}P\{^1H\}$ NMR (121 MHz, δ/ppm in benzene-d_6): 25.09 (s), −4.56 (s). Anal. Calcd for $C_{35}H_{56}N_2P_2$: C, 74.17; H, 9.96; N, 4.94. Found: C, 73.17; H, 10.10; N, 4.28.

Preparation of $Fe(NpNP^{iPr})Br$. Under a dinitrogen atmosphere, $FeBr_2(THF)_2$ (3.01 g, 8.41 mmol) was added to 40 mL of a solution of $LiNpNP^{iPr}$ in Et_2O (4.83 g, 8.43 mmol). The mixture was stirred at room temperature for 3 h. The reaction mixture was filtered through Celite to give a yellow solution. Volatiles were removed in vacuo, and 30 mL of *n*-pentane was added to the mixture, which was then stored in the freezer at −35 °C. The compound $FeBr(NpNP^{iPr})$ was obtained as a yellow powder (5.18 g, 7.38 mmol, 87% yield). Several recrystallizations of $FeBr(NpNP^{iPr})$ from *n*-pentane gave pale-yellow single crystals suitable for X-ray analysis. ^1H NMR (300 MHz, δ/ppm in benzene-d_6): −146.81, −22.66, −9.90, −8.82, −5.38, −4.44, −2.37, 1.12, 3.27, 4.72, 8.13, 12.41, 13.28, 19.16, 24.22, 28.36, 30.25, 33.34, 46.49, 87.88, 106.99. μ_{eff} = 5.06μ_B (Evans method). Anal. Calcd for $C_{35}H_{55}BrFeN_2P_2$: C, 61.25; H, 7.71; N, 4.46. Found: C, 61.09; H, 7.18; N, 4.38.

Preparation of $[Fe(NpNP^{iPr})]_2(\mu\text{-}N_2)$. Under a dinitrogen atmosphere, KC_8 (100 mg, 0.74 mmol) was added to a slurry of $FeBr(NpNP^{iPr})$ (500 mg, 0.71 mmol) in *n*-pentane (10 mL). The reaction mixture was stored overnight at −35 °C and then stirred for 1 day at room temperature to yield a dark-red solution. Graphite and KBr were removed by filtration, and the solvent was reduced in volume to 1 mL in vacuo. After the solution was stored at −35 °C for a few days, black needle crystals were obtained (51 mg, 13% yield). The desired crystals for elemental analysis were also obtained from Et_2O, and the corresponding crystal structure is shown in Figure S9 in the Supporting Information. ^1H NMR (300 MHz, δ/ppm in benzene-d_6): −37.56, −18.01, 10.53, 0.59, 0.87, 1.22, 17.29, 18.12, 19.77, 23.40, 33.73, 39.52, 46.89, 148.29. μ_{eff} = 6.92μ_B (Evans method, in benzene-d_6). Anal. Calcd for $C_{70}H_{110}Fe_2N_6P_4{\cdot}2(C_4H_{10}O)$: C, 66.00; H, 9.23; N, 5.92. Found: C, 65.69; H, 8.89; N, 5.68.

■ ASSOCIATED CONTENT

Supporting Information

^1H and ^{31}P NMR spectra of $LiNpNP^{iPr}$ and $HNpNP^{iPr}$; crystal structures of $LiNpNP^{iPr}$, $HNpNP^{iPr}$, $FeBr(NpNP^{iPr})$, and $[Fe(NpNP^{iPr})]_2(\mu\text{-}N_2)$ (CIF); detailed information on the X-ray crystal analysis; and computational results. The Supporting Information is available free of charge on the ACS Publications website at DOI: 10.1021/acs.inorgchem.5b00536.

■ AUTHOR INFORMATION

Corresponding Authors

*E-mail: masuda.hideki@nitech.ac.jp.

*E-mail: fryzuk@chem.ubc.ca.

Notes

The authors declare no competing financial interest.

■ ACKNOWLEDGMENTS

We gratefully acknowledge support for this work by a Grant-in-Aid for Scientific Research from the Ministry of Education, Culture, Sports, Science and Technology of Japan and by the "Strategic Young Researcher Overseas Visits Program for Accelerating Brain Circulation" of the Japan Society for the Promotion of Science. We also thank Toyota Motor Corporation for financial support and for many helpful discussions. The NSERC of Canada is also acknowledged for support in the form of a Discovery Grant to M.D.F. We thank Prof. Ko Mibu (NIT) for technical assistance.

■ REFERENCES

(1) Allen, A. D.; Senoff, C. V. *Chem. Commun.* **1965**, 621−622.

(2) (a) Hidai, M.; Mizobe, Y. *Chem. Rev.* **1995**, *95*, 1115−1133. (b) Chirik, P. J. *Dalton Trans.* **2007**, 16−25. (c) Fryzuk, M. D. *Chem. Commun.* **2013**, *49*, 4866−4868. (d) Hidai, M. *Coord. Chem. Rev.* **1999**, *185*−*186*, 99−108. (e) Chatt, J.; Dilworth, J. R.; Richards, R. L. *Chem. Rev.* **1978**, *78*, 589−625.

(3) (a) Einsle, O.; Tezcan, F. A.; Andrade, S. L. A.; Schmid, B.; Yoshida, M.; Howard, J. B.; Rees, D. C. *Science* **2002**, *297*, 1696−1700. (b) Lancaster, K. M.; Roemelt, M.; Ettenhuber, P.; Hu, Y.; Ribbe, M. W.; Neese, F.; Bergmann, U.; DeBeer, S. *Science* **2011**, *334*, 974−977. (c) Spatzal, T.; Aksoyoglu, M.; Zhang, L.; Andrade, S. L. A.; Schleicher, E.; Weber, S.; Rees, D. C.; Einsle, O. *Science* **2011**, *334*, 940.

(4) (a) Chatt, J.; Pearman, A. J.; Richards, R. L. *Nature* **1975**, *253*, 39−40. (b) Chatt, J.; Pearman, A. J.; Richards, R. L. *J. Chem. Soc., Dalton Trans.* **1977**, 1852−1860. (c) Chatt, J.; Dilworth, J. R. *Chem. Commun.* **1975**, 983−984. (d) George, T. M.; Tisdale, C. *J. Am. Chem. Soc.* **1985**, *107*, 5157−5159. (e) Ogawa, T.; Kajita, Y.; Wasada-Tsutsui, Y.; Wasada, H.; Masuda, H. *Inorg. Chem.* **2013**, *52*, 182−195.

(5) (a) Yandulov, D. V.; Schrock, R. R. *Science* **2003**, *301*, 76−78. (b) Schrock, R. R. *Acc. Chem. Res.* **2005**, *38*, 955−962.

(6) Arashiba, K.; Miyake, Y.; Nishibayashi, Y. *Nat. Chem.* **2011**, *3*, 120−125.

(7) (a) Russell, S. K.; Darmon, J. M.; Lobkovsky, E.; Chirik, P. J. *Inorg. Chem.* **2010**, *49*, 2782−2792. (b) Trovitch, R. J.; Lobkovsky, E.; Chirik, P. J. *Inorg. Chem.* **2006**, *45*, 7252−7260. (c) Hoyt, J. M.; Sylvester, K. T.; Semproni, S. P.; Chirik, P. J. *J. Am. Chem. Soc.* **2013**, *135*, 4862−4877. (d) Bowman, A. C.; Milsmann, C.; Atienza, C. C. H.; Lobkovsky, E.; Wieghardt, K.; Chirik, P. J. *J. Am. Chem. Soc.* **2010**, *132*, 1676−1684.

(8) (a) Holland, P. L. *Dalton Trans.* **2010**, *39*, 5415−5425. (b) Smith, J. M.; Lachicotte, R. J.; Pittard, K. A.; Cundari, T. R.; Lukat-Rodgers, G.; Rodgers, K. R.; Holland, P. L. *J. Am. Chem. Soc.* **2001**, *123*, 9222−

DOI: 10.1021/acs.inorgchem.5b00536
Inorg. Chem. 2015, 54, 9271−9281

9223. (c) Rodriguez, M. M.; Bill, E.; Brennessel, W. W.; Holland, P. L. *Science* **2011**, *334*, 780−783. (d) Smith, J. M.; Sadique, A. R.; Cundari, T. R.; Rodgers, K. R.; Lukat-Rodgers, G.; Lachicotte, R. J.; Flaschenriem, C. J.; Vela, J.; Holland, P. L. *J. Am. Chem. Soc.* **2006**, *128*, 756−769. (e) Holland, P. L. *Can. J. Chem.* **2005**, *83*, 296−301. (f) Stoian, S. A.; Vela, J.; Smith, J. M.; Sadique, A. R.; Holland, P. L.; Münck, E.; Bominaar, E. L. *J. Am. Chem. Soc.* **2006**, *128*, 10181−10192. (g) Lee, Y.; Sloane, F. T.; Blondin, G.; Abboud, K. A.; García-Serres, R.; Murray, L. J. *Angew. Chem., Int. Ed.* **2015**, *54*, 1499−1503.

(9) (a) Moret, M.-E.; Peters, J. C. *J. Am. Chem. Soc.* **2011**, *133*, 18118−18121. (b) Takaoka, A.; Mankad, N. P.; Peters, J. C. *J. Am. Chem. Soc.* **2011**, *133*, 8440−8443. (c) Whited, M. T.; Mankad, N. P.; Lee, Y.; Oblad, P. F.; Peters, J. C. *Inorg. Chem.* **2009**, *48*, 2507−2517. (d) Lee, Y.; Mankad, N. P.; Peters, J. C. *Nat. Chem.* **2010**, *2*, 558−565. (e) Anderson, J. S.; Rittle, J.; Peters, J. C. *Nature* **2013**, *501*, 84−88. (f) Creutz, S. E.; Peters, J. C. *J. Am. Chem. Soc.* **2014**, *136*, 1105−1115. (g) Suess, D. L. M.; Peters, J. C. *J. Am. Chem. Soc.* **2013**, *135*, 4938−4941. (h) Betley, T. A.; Peters, J. C. *J. Am. Chem. Soc.* **2003**, *125*, 10782−10783. (i) Hendrich, M. P.; Gunderson, W.; Behan, R. K.; Green, M. T.; Mehn, M. P.; Betley, T. A.; Lu, C. C.; Peters, J. C. *Proc. Natl. Acad. Sci. U.S.A.* **2006**, *103*, 17107−17112.

(10) Spencer, L. P.; Altwer, R.; Wei, P.; Gelmini, L.; Gauld, J.; Stephan, D. W. *Organometallics* **2003**, *22*, 3841−3854.

(11) (a) Keim, W.; Killat, S.; Nobile, C. F.; Suranna, G. P.; Englert, U.; Wang, R.; Mecking, S.; Schröder, D. L. *J. Organomet. Chem.* **2002**, *662*, 150−171. (b) Zhu, T.; Wambach, T. C.; Fryzuk, M. D. *Inorg. Chem.* **2011**, *50*, 11212−11221. (c) Wambach, T. C.; Ahn, J. M.; Patrick, B. O.; Fryzuk, M. D. *Organometallics* **2013**, *32*, 4431−4439.

(12) Ogawa, T.; Suzuki, T.; Hein, N. M.; Pick, F. S.; Fryzuk, M. D. *Dalton Trans.* **2015**, *44*, 54−57.

(13) Vela, J.; Cirera, J.; Smith, J. M.; Lachicotte, R. J.; Flaschenriem, C. J.; Alvarez, S.; Holland, P. L. *Inorg. Chem.* **2007**, *46*, 60−71.

(14) Weintrob, E. C.; Tofan, D.; Bercaw, J. E. *Inorg. Chem.* **2009**, *48*, 3808−3813.

(15) (a) Schubert, E. M. *J. Chem. Educ.* **1992**, *69*, 62. (b) Evans, D. F. *J. Chem. Soc.* **1959**, 2003−2005.

(16) Betley, T. A.; Peters, J. C. *J. Am. Chem. Soc.* **2004**, *126*, 6252−6254.

(17) Mankad, N. P.; Whited, M. T.; Peters, J. C. *Angew. Chem., Int. Ed.* **2007**, *46*, 5768−5771.

(18) Rose, R. P.; Jones, C.; Schulten, C.; Aldridge, S.; Stasch, A. *Chem.—Eur. J.* **2008**, *14*, 8477−8480.

(19) (a) Chomitz, W. A.; Arnold, J. *Chem. Commun.* **2007**, 4797−4799. (b) Chomitz, W. A.; Arnold, J. *Dalton Trans.* **2009**, 1714−1720.

(20) Altomare, A.; Cascarano, G.; Giacovazzo, C.; Guagliardi, A.; Burla, M. C.; Polidori, G.; Camalli, M. *J. Appl. Crystallogr.* **1994**, *27*, 435.

(21) Sheldrick, G. M. *SHELXL97*; University of Göttingen: Göttingen, Germany, 1997.

(22) Cromer, D. T.; Waber, J. T. *International Tables for X-ray Crystallography, Vol. IV*; Ibers, J. A., Hamilton, W. C., Eds.; Kynoch Press: Birmingham, U.K., 1974; Table 2.2A.

(23) Ibers, J. A.; Hamilton, W. C. *Acta Crystallogr.* **1964**, *17*, 781−782.

(24) Creagh, D. C.; McAuley, W. J. In *International Tables for Crystallography, Vol. C*; Wilson, A. J. C., Ed.; Kluwer: Dordrecht, The Netherlands, 1992; Table 4.2.6.8, pp 219−222.

(25) Creagh, D. C.; Hubbell, J. H. In *International Tables for Crystallography, Vol. C*; Wilson, A. J. C., Ed.; Kluwer: Dordrecht, The Netherlands, 1992; Table 4.2.4.3, pp 200−206.

(26) Bergbreiter, D. W.; Killough, J. M. *J. Am. Chem. Soc.* **1978**, *100*, 2126−2134.

(27) Al-Benna, S.; Sarsfield, M. J.; Thornton-Pett, M.; Ormsby, D. L.; Maddox, P. J.; Brès, P.; Bochmann, M. *J. Chem. Soc., Dalton Trans.* **2000**, 4247−4257.

(28) Becke, A. D. *J. Chem. Phys.* **1993**, *98*, 5648−5652.

(29) (a) Wachters, A. J. H. *J. Chem. Phys.* **1970**, *52*, 1033−1036. (b) Raghavachari, K.; Trucks, G. W. *J. Chem. Phys.* **1989**, *91*, 1062−1065. (c) McLean, A. D.; Chandler, G. S. *J. Chem. Phys.* **1980**, *72*, 5639−5648. (d) Raghavachari, K.; Binkley, J. S.; Seeger, R.; Pople, J. A. *J. Chem. Phys.* **1980**, *72*, 650−654. (e) Hehre, W. J.; Ditchfield, R.; Pople, J. A. *J. Chem. Phys.* **1972**, *56*, 2257−2261. (f) Hariharan, P. C.; Pople, J. A. *Theor. Chem. Acc.* **1973**, *28*, 213−222.

(30) Reed, A. E.; Weinstock, R. B.; Weinhold, F. *J. Chem. Phys.* **1985**, *83*, 735−746.

(31) Mulliken, R. S. *J. Chem. Phys.* **1955**, *23*, 1833−1840.

(32) (a) Weinhold, F.; Landis, C. R. *Valency and Bonding: A Natural Bond Orbital Donor−Acceptor Perspective*; Cambridge University Press: Cambridge, U.K., 2005. (b) Reed, A. E.; Curtiss, L. A.; Weinhold, F. *Chem. Rev.* **1988**, *88*, 899−926.

(33) Frisch, M. J.; Trucks, G. W.; Schlegel, H. B.; Scuseria, G. E.; Robb, M. A.; Cheeseman, J. R.; Scalmani, G.; Barone, V.; Mennucci, B.; Petersson, G. A.; Nakatsuji, H.; Caricato, M.; Li, X.; Hratchian, H. P.; Izmaylov, A. F.; Bloino, J.; Zheng, G.; Sonnenberg, J. L.; Hada, M.; Ehara, M.; Toyota, K.; Fukuda, R.; Hasegawa, J.; Ishida, M.; Nakajima, T.; Honda, Y.; Kitao, O.; Nakai, H.; Vreven, T.; Montgomery, J. A., Jr.; Peralta, J. E.; Ogliaro, F.; Bearpark, M.; Heyd, J. J.; Brothers, E.; Kudin, K. N.; Staroverov, V. N.; Kobayashi, R.; Normand, J.; Raghavachari, K.; Rendell, A.; Burant, J. C.; Iyengar, S. S.; Tomasi, J.; Cossi, M.; Rega, N.; Millam, J. M.; Klene, M.; Knox, J. E.; Cross, J. B.; Bakken, V.; Adamo, C.; Jaramillo, J.; Gomperts, R.; Stratmann, R. E.; Yazyev, O.; Austin, A. J.; Cammi, R.; Pomelli, C.; Ochterski, J. W.; Martin, R. L.; Morokuma, K.; Zakrzewski, V. G.; Voth, G. A.; Salvador, P.; Dannenberg, J. J.; Dapprich, S.; Daniels, A. D.; Farkas, Ö.; Foresman, J. B.; Ortiz, J. V.; Cioslowski, J.; Fox, D. J. *Gaussian 09*, revision D.01; Gaussian, Inc.: Wallingford, CT, 2009.

(34) (a) Wasada, H.; Tsutsui, Y. *Bull. Coll. Gen. Educ.* **1996**, *33*, 145−158. (b) Takahashi, I.; Wasada, H.; Tsutsui, Y. *MOVIEW: Program of Nagoya University Information Technology Center Representing Molecular Orbitals and Electron Density Maps by Isosurfaces*.

DOI: 10.1021/acs.inorgchem.5b00536
Inorg. Chem. 2015, 54, 9271−9281